0026-895X/06/6903-833–845$20.00
MOLECULAR PHARMACOLOGY
Copyright © 2006 The American Society for Pharmacology and Experimental Therapeutics
Mol Pharmacol 69:833–845, 2006

Vol. 69, No. 3
16998/3084529
Printed in U.S.A.

Insulin-Like Growth Factor Binding Protein-2: Contributions of the C-Terminal Domain to Insulin-Like Growth Factor-1 Binding

Megan M. Kibbey, Mark J. Jameson, Erin M. Eaton, and Steven A. Rosenzweig

Department of Cell and Molecular Pharmacology and Experimental Therapeutics and Hollings Cancer Center, Medical University of South Carolina, Charleston, South Carolina (M.M.K., E.M.E., S.A.R.); and Department of Otolaryngology-Head and Neck Surgery, University of Virginia Health System, Charlottesville, Virginia (M.J.J.)

Received July 21, 2005; accepted November 23, 2005

ABSTRACT

Signaling by the insulin-like growth factor (IGF)-1 receptor (IGF-1R) has been implicated in the promotion and aggressiveness of breast, prostate, colorectal, and lung cancers. The IGF binding proteins (IGFBPs) represent a class of natural IGF antagonists that bind to and sequester IGF-1/2 from the IGF-1R, making them attractive candidates as therapeutics for cancer prevention and control. Recombinant human IGFBP-2 significantly attenuated IGF-1-stimulated MCF-7 cell proliferation with coaddition of 20 or 100 nM IGFBP-2 (50 or 80% inhibition, respectively). We previously identified IGF-1 contact sites both upstream and downstream of the CWCV motif (residues 247–250) in human IGFBP-2 (*J Biol Chem* **276:**2880–2889, 2001). To further test their contributions to IGFBP-2 function, the single tryptophan in human IGFBP-2, Trp-248, was selectively cleaved with 2-(2′nitrophenylsulfenyl)-3-methyl-3 bromoindolenine (BNPS-skatole) and the BNPS-skatole products IGFBP-$2_{1–248}$ and IGFBP-$2_{249–289}$ as well as IGFBP-$2_{1–190}$ were expressed as glutathione *S*-transferase-fusion proteins and purified. Based on competition binding analysis, deletion of residues 249 to 289 caused an ~20-fold decrease in IGF-1 binding affinity (IGFBP-2 EC_{50} = 0.35 nM and IGFBP-$2_{1–248}$ = 7 nM). Removal of the remainder of the C-terminal domain had no further effect on affinity (IGFBP-$2_{1–190}$ EC_{50} = 9.2 nM). In kinetic assays, IGFBP-$2_{1–248}$ and IGFBP-$2_{1–190}$ exhibited more rapid association and dissociation rates than full-length IGFBP-2. These results confirm that regions upstream and downstream of the CWCV motif participate in IGF-1 binding. They further support the development of full-length IGFBP-2 as a cancer therapeutic.

Insulin-like growth factor (IGF)-1 is a well recognized survival factor thought to play a key role in antiapoptotic and mitogenic signaling in cancer. The IGF-1 receptor (IGF-1R) acting through phosphoinositide 3-kinase/Akt signaling pathways has been linked to enhanced cell growth and tumorigenesis (Rosenzweig, 2004). In this regard, the IGF binding proteins (IGFBPs) are a class of six soluble proteins exhibiting high affinity for the IGFs capable of reducing IGF-1R activation via sequestration (Rosenzweig, 2004). Over the past few years, studies have demonstrated that IGFBP-3 (Imai et al., 2000) and IGFBP-2 (Dong et al., 2002) have intrinsic biologic activities independent of their IGF sequestration abilities. This is further complicated with respect to IGFBP-2, which has been reported to have opposite effects on normal versus cancer cells (Moore et al., 2003). In addition, a number of in vitro studies using colon, adrenal, and prostate cancer cell lines have revealed a positive association between cell proliferation and IGFBP-2 expression (Hoeflich et al., 2001). Therefore, one must test the actions of the IGFBPs in each system to determine whether they exhibit IGF-1-dependent or independent effects.

The six IGFBPs each contain three distinct domains. The N and C termini are highly conserved and contain 16 to 18

This work was supported, in part, by National Institutes of Health Grant CA-78887 and Department of Defense grant N6311601MD10004 to Hollings Cancer Center (to S.A.R.). M.M.K. was supported by National Research Service Award 5F30-DE015249 from the National Institute of Dental and Craniofacial Research and by the Dental Medicine Scientist Training Program, Colleges of Dental Medicine and Graduate Studies, Medical University of South Carolina. E.M.E. was supported by National Institutes of Health postdoctoral training grant T32-HL07260.

This work was presented in part at the 87th Annual Meeting of the Endocrine Society, June 2004, New Orleans, LA.

Article, publication date, and citation information can be found at http://molpharm.aspetjournals.org.

doi:10.1124/mol.105.016998.

ABBREVIATIONS: IGF, insulin-like growth factor; IGF-1R, insulin-like growth factor-1 receptor; IGFBP, insulin-like growth factor binding protein; BNPS-skatole, 2-(2′nitrophenylsulfenyl)-3-methyl-3 bromoindolenine; GST, glutathione *S*-transferase; CHO, Chinese hamster ovary; DHFR, dihydrofolate reductase; HRP, horseradish peroxidase; CM, conditioned medium; HPLC, high-performance liquid chromatography; RP-HPLC, reverse phase-high-performance liquid chromatography; TFA, trifluoroacetic acid; PVDF, polyvinylidene difluoride; MALDI-TOF, matrix-assisted laser desorption ionization/time of flight; SDS, sodium dodecyl sulfate; PEG, polyethylene glycol; BSA, bovine serum albumin; MS, mass spectrometry; TBS, Tris-buffered saline; PCR, polymerase chain reaction; PAGE, polyacrylamide gel electrophoresis.

cysteine residues, forming eight to nine disulfide bonds (Rosenzweig, 2004). Based on their disulfide bonding pattern, the IGFBPs are thyroglobulin type-1 domain homologs (Guncar et al., 1999). NMR spectroscopy and X-ray crystallography have confirmed these domains in IGFBP-6 (Bach et al., 2005) and IGFBP-1 (Sala et al., 2005), respectively. Notwithstanding their structural homologies, a consensus understanding of the IGF binding domain on the IGFBPs remains elusive. Previous studies indicated that a key IGF-1 binding site on IGFBP-2 is located within its C terminus (Wang et al., 1988; Ho and Baxter, 1997; Forbes et al., 1998; Shand et al., 2003; Carrick et al., 2005; Mark et al., 2005), whereas both the N (Kalus et al., 1998; Imai et al., 2000; Zeslawski et al., 2001; Hong et al., 2002) and C termini (Galanis et al., 2001) of IGFBP-3 have been implicated in IGF binding. Studies have also shown the need for both the N and C termini of IGFBP-2 (Carrick et al., 2001), IGFBP-3 (Payet et al., 2003), and IGFBP-6 (Bach et al., 2005) for IGF-1/2 binding.

As an initial step in designing small molecular weight, IGFBP-based agents that antagonize IGF action, we are analyzing the structure of the IGF binding site on IGFBP-2. Photoaffinity labeling experiments revealed the photoincorporation of two different Gly-1–labeled IGF-1 photoprobes at two C-terminal sites within human IGFBP-2 (212–227 and 266–287), on either side of its CWCV motif (residues 247–250; Fig. 1) (Horney et al., 2001). These findings were consistent with other reports (Forbes et al., 1998; Carrick et al., 2001; Shand et al., 2003), indicating a role for the C-terminal thyroglobulin type-1 domain fold in IGF binding (see legend to Fig. 1 for details). Recent NMR analysis of IGFBP-6 could not resolve the distal C terminus, suggesting it lacked structure and was probably unimportant in IGF binding (Bach et al., 2005). To resolve whether residues downstream of the CWCV motif of IGFBP-2 contribute to IGF binding, we used the tryptophan-specific cleavage reagent BNPS-skatole (Fontana, 1972). This reagent is ideally suited for use with IGFBP-2 because it contains a single tryptophan residue, located within its CWCV motif. Furthermore, this cleavage site exists outside the disulfide bonding pattern, essential to maintaining the tertiary structure of this protein. To determine the affinity of the BNPS-skatole products, we have expressed and purified IGFBP-$2_{1–248}$ and IGFBP-$2_{249–289}$ as well as IGFBP-$2_{1–190}$ as N-terminal GST-fusion proteins in *Escherichia coli*. In addition, human IGFBP-2 with an N-terminal hexahistidine tag (6His) was expressed in *E. coli* as a control.

In this study, we generated and purified recombinant IGFBP-2, exhibiting a high affinity for IGF-1 (K_D = 150 pM). Treatment of MCF-7 human breast cancer cells with recombinant IGFBP-2 inhibited both IGF-1-stimulated and basal cell growth. Cleavage of IGFBP-2 with BNPS-skatole resulted in the predicted products. The functionality of these cleavage products was further tested using recombinant IGFBP-$2_{1–248}$ and IGFBP-$2_{249–289}$. Recombinant IGFBP-$2_{1–190}$ had similar IGF binding properties to IGFBP-$2_{1–248}$ with lower efficacy in blocking IGF-1 binding to the receptor. 6His-IGFBP-2 was generated and shown to have equivalent activities compared with human IGFBP-2 expressed in CHO cells. These data indicate that both the proximal and distal regions of the C terminus of IGFBP-2 contribute to the structural information important for high-affinity IGF-1 binding.

Materials and Methods

Materials. Human recombinant IGF-1 was generously provided by Genentech (South San Francisco, CA). The cDNA encoding human IGFBP-2 (Binkert et al., 1989) was obtained from Dr. Jörg Landwehr (Roche Biotech, Basel, Switzerland). DHFR$^-$ CHO cells and the pMT2 mDHFR expression vector were provided by Dr. David Kurtz (Medical University of South Carolina, Charleston, SC). Human IGF-2 was obtained from GroPep (Adelaide, Australia). HPLC columns were from Vydac Instruments (Hesperia, CA). Tissue culture medium was obtained from Sigma-Aldrich (St. Louis, MO). Tris(2-carboxyethyl) phosphine hydrochloride and HRP-NeutrAvidin were obtained from Pierce Chemical (Rockford, IL). Restriction enzymes (EcoRI, BamHI, HindIII, SalI, SphI, and XbaI) and restriction buffer were obtained from New England Biolabs (Beverly, MA). All oligonucleotides were purchased from Integrated DNA Technologies (Coralville, IA). All other materials were of reagent grade.

Transfection of DHFR$^-$ CHO Cells. The cDNA for human IGFBP-2 (Feyen et al., 1991) was excised from pTZ18R by digestion with EcoRI and ligated into the EcoRI site of pCMV. DHFR$^-$ CHO cells (clone DG44) were transfected with 30 μg of pCMV-IGFBP-2 and 2 μg of pMT2 containing mDHFR (Kaufman and Sharp, 1982) using the calcium phosphate method (Sambrook et al., 1989). After 24 h, plates were split 1:4 into nucleoside-free Ham's F-12 medium containing 10% calf serum and maintained until colony formation.

Fig. 1. Primary sequences of the C-terminal domains of human, bovine, and rat IGBP-2 and human IGFBP-1. Boxed sequences denote consensus CWCV motifs. Gray box encompasses the thyroglobulin type-1 domain. Underlines in human IGFBP-2 are sites (212–227 and 266–287) photoaffinity labeled with IGF-1 (Horney et al., 2001). Open arrowhead indicates the location of the BNPS-skatole cleavage site. Underlining in bovine IGFBP-2 denotes the site defined for IGF binding (residues 222–236) (Forbes et al., 1998). Dark arrowheads designate residues (Gly-211 and Glu-217) mutated in rat IGFBP-2 (Shand et al., 2003) resulting in reduced IGF-1 binding activity. Gray arrowhead in human IGFBP-1 denotes His-213 shown to bind to Fe^{2+}, which in turn antagonized IGF-2 binding (Sala et al., 2005).

Individual clones were isolated by discrete trypsinization and were subsequently expanded and amplified by splitting into successively higher concentrations of methotrexate. An appropriate clone (CHO-IGFBP2) was selected based on its high level of IGFBP-2 secretion into serum-free medium over a 24-h window as detected by Coomassie Blue staining and confirmed by anti-IGFBP-2 immunoblot. This clone was maintained at 100 mg/l methotrexate to preserve amplification of the expressed genes.

Purification of IGFBP-2. CHO-IGFBP-2 cells were grown to confluence in roller bottles and subjected to a weekly cycle of 3 days of growth in serum-containing medium followed by 4 days in serum-free medium. Batches of conditioned medium (CM; 400–600 ml) were acidified to pH 3 to 4 with glacial acetic acid, dialyzed, followed by dialysis in distilled water using Spectra/Por 4 membranes (Spectrum, Laguna Hills, CA; 12,000–14,000 molecular weight cut-off) to remove salt and IGF-1, and lyophilized. IGF-1-Sepharose columns were prepared using CH-Sepharose (Amersham Biosciences Inc., Piscataway, NJ) according to the manufacturer's instructions.

Dialyzed, lyophilized CM was dissolved in 40 to 45 ml of 50 mM HEPES, pH 7.4, containing 150 mM NaCl (buffer A). Insoluble material was removed by centrifugation at 3000*g* for 20 min. Two milliliters of IGF-1-Sepharose in buffer A was added, and the slurry was incubated overnight at 4°C with agitation. The column was subsequently washed with 100 ml of buffer A followed by 50 ml of 10% buffer A. Proteins bound to the column were eluted with 15 ml of 0.5 M acetic acid, dried in vacuo using a SpeedVac concentrator (Thermo Electron, Waltham, MA), and stored at −20°C until further purification by reversed phase HPLC (RP-HPLC) on a C4 column equilibrated in 0.1% trifluoroacetic acid (TFA) and eluted with a gradient of acetonitrile.

Matrix-Assisted Laser Desorption Ionization/Time-of-Flight Mass Spectrometry. Proteins were reduced and alkylated using the water-soluble tris-alkylphosphine tris(2-carboxyethyl) phosphine as the reducing agent and 4-vinylpyridine (Sigma-Aldrich) as the alkylating agent as reported previously (Horney et al., 2001). Aliquots (1 ml) of each sample to be analyzed were mixed with a 50 mM solution of α-cyano-4-hydroxycinnamic acid dissolved in 70% acetonitrile [1:5 (v/v) protein/matrix; Sigma-Aldrich], and 1 μl of this mixture was placed on a gold-coated, stainless steel sample plate and air-dried. The samples were analyzed using an Applied Biosystems (Foster City, CA) Voyager-DE MALDI-TOF mass spectrometer equipped with a 337-nm nitrogen laser. A delayed extraction source was operated in linear mode (1.2-m ion flight path; 20-kV accelerating voltage) to acquire the mass spectra. Between 100 and 120 mass scans were averaged to obtain one mass spectrum. Instrumental resolution in linear mode with delayed extraction was approximately 700 (full width at half maximum) at *m/z* 1297.5. External mass calibration was performed using angiotensin I (mol. wt. 1297.5) and adrenocorticotropic hormone clip 7-38 (mol. wt. 3660.2) as standards. Mass accuracy was ± 2 Da/1000 Da.

Immunoblot Analysis. Samples were dissolved in SDS sample buffer with or without dithiothreitol and resolved on 12.5% SDS-polyacrylamide gels using a Hoeffer apparatus (Hoeffer, San Francisco, CA). Afterelectrophoresis, proteins were transferred to nitrocellulose. The membranes and were blocked for 20 min with bovine lacto-transfer technique optimizer [5% (w/v) milk protein in Tris-buffered saline with Tween, 10 mM Tris, pH 8.0, containing 150 mM NaCl and 0.05% Tween 20], incubated with a commercial antiserum against intact bovine IGFBP-2 from Upstate Biotechnology (Charlottesville, VA) or with an anti-C-terminal antiserum (Santa Cruz Biotechnology, Inc., Santa Cruz, CA). Blots were developed and quantified with goat anti-rabbit HRP-conjugated antibodies from Chemicon International (Temecula, CA) and developed with the enhanced chemiluminescence reagent from Amersham Biosciences Inc.

MCF-7 Cell Proliferation Assay. MCF-7 cells were grown in 24-well plates in phenol red-free RPMI 1640 medium containing 10% fetal bovine serum. After a 24-h serum starvation, they were washed with phosphate-buffered saline and stimulated with a range of IGF-1 doses, as indicated. IGFBP-2 was added at 20 or 100 nM concentrations. The wash and treatments were repeated at 48 h, and the cells were harvested and counted at 96 h. Average cell numbers as a percentage of control (unstimulated cells minus IGFBP-2) for triplicate wells was determined.

IGFBP-2 Binding Assay. IGFBP-2 binding assays were carried out using polyethylene glycol (PEG) precipitation and centrifugation (McCusker et al., 1988). IGFBP-2 (1 or 4 ng), 6His-IGFBP-2 (4 ng), IGFBP-$2_{1–248}$ (100 ng), or IGFBP-$2_{1–190}$ (100 ng) was combined with various concentrations of IGF-1 ranging from 30 fM to 100 nM in binding assay buffer (100 mM HEPES, pH 7.4, 44 mM $NaHCO_3$, 0.01% BSA, 0.01% Triton X-100, and 0.02% NaN_3) followed by addition of 10 nCi of ^{125}I-IGF-1 (Amersham Biosciences Inc.). After a 4-h incubation at 23°C (or overnight incubation at 4°C), 250 μl of 0.5% bovine gamma globulin was added followed by 500 μl of 25% PEG (average mol. wt. 8000; Sigma-Aldrich). The samples were incubated for 10 min at 23°C and centrifuged 3 min at 13,000 rpm. The pellets were washed with 1 ml of 6.25% PEG, and bound radioactivity was quantified in a Compugamma spectrometer (LKB-Wallac, Turku, Finland). Counts bound in the presence of 1 μM IGF-1 (nonspecific binding) were subtracted to obtain specific binding.

BNPS-Skatole Cleavage of IGFBP-2. Fifty micrograms of IGFBP-2 was dissolved in 0.1 M acetic acid. BNPS-skatole (Pierce Chemical) was dissolved in 1.5 ml of glacial acetic acid (0.333 mg/ml), and 150 μl was mixed with 50 μl of IGFBP-2. The reaction mixture was incubated in a hybridization oven for 3 h at 47°C in the dark. For extraction, 200 μl of water was added to the reaction mixture, which was vortexed and centrifuged at 13,000 rpm for 3 min. The supernatant was saved, and the pellet was re-extracted in 500 μl of 0.1 M acetic acid, vortexed, and centrifuged as described above. The supernatants were combined, vortexed, centrifuged, and dried in vacuo in a SpeedVac concentrator. The dried protein was re-extracted in 200 μl of 0.1 M acetic acid, followed by vortexing and centrifugation. The supernatant was dried in vacuo and stored at −20°C until further use.

Analysis of BNPS-Skatole Cleavage Reaction Products. The BNPS-skatole reaction products from a 300-μg reaction were reconstituted in 100 μl of 0.1% acetic acid, 220 μl of 0.5% TFA, and 1 μl of 100% TFA. This was then injected onto a C4 column equilibrated in 0.1% TFA at a flow rate of 1 ml/min. After 10 min, a linear gradient of 0 to 60% acetonitrile was developed over 60 min to elute the reaction products. Fractions from each peak were collected and dried in vacuo, boiled in SDS sample buffer, and resolved on a 12.5% nonreducing polyacrylamide gel. Proteins were transferred to an Immobilon-Psq microporous polyvinylidene difluoride (PVDF) membrane (Millipore Corporation, Billerica, MA) as described above. The membrane was briefly rinsed with distilled H_2O, saturated with 100% methanol, and stained with Coomassie Brilliant Blue (0.1% Coomassie Blue R-250 in 1% acetic acid, 40% methanol, and 12.5% trichloroacetic acid) at 23°C for 30 min. The membrane was destained in 50% methanol. Bands were excised and sequenced by Edman degradation, using a gas-phase sequencer (ABI 377; Applied Biosystems), in the Protein Sequencing and Peptide Synthesis Facility, Biotechnology Resource Laboratory (Medical University of South Carolina).

MALDI-TOF MS of BNPS-Skatole Reaction Products. Dried HPLC fractions of the BNPS-skatole reaction products were dissolved in 30 μl of 0.1% TFA containing 60% acetonitrile. Then, 0.5 μl-aliquots of each fraction or of recombinant protein was mixed with 1.5 μl of 50 mM α-cyano-4-hydroxycinnamic acid in 0.1% TFA and 70% acetonitrile. The mixture was spotted onto a gold-coated, stainless steel plate, air-dried, and analyzed using an Applied Biosystems Voyager-DE MALDI-TOF mass spectrometer as detailed above. External mass calibrations were performed using angiotensin I (1297.5 Da), bovine insulin (5734.54 Da), horse apomyoglobin (16,952.56 Da), and *E. coli* thioredoxin (11,674.48 Da). Mass accuracy was ± 0.1%.

Ligand Blot Analysis. In preparation for ligand blot analysis, samples were boiled in SDS sample buffer (125 mM Tris, pH 6.95, containing 4% SDS, 10 mM EDTA, 15% sucrose, and 0.01% bromphenol blue) and resolved on a 12.5% nonreducing polyacrylamide gel. Proteins were transferred to nitrocellulose (MSI Separations, Minnetonka, MN) with a TE-70 SemiPhor apparatus (Hoeffer) using a one-buffer system (48 mM Tris, 39 mM glycine, 0.0375% SDS, and 20% methanol). Transfers were performed at 23°C for 60 min using a constant current of 1.2 mA/cm^2. The nitrocellulose was then washed at 23°C for 10 min in Tris-buffered saline (TBS; 150 mM NaCl, 10 mM Tris-HCl, and 0.5 g/liter NaN_3, pH 7.4) containing 3% Nonidet P-40, 1 h in TBS containing 0.2% gelatin and 5 min in TBS containing 0.1% Tween 20. The nitrocellulose was incubated in TBS with 0.1% Tween 20, 0.5% BSA containing 0.4 μg of tetrabiotinylated-IGF-1, $N^{\epsilon Lys\text{-}65/68}$(biotin)-IGF-1, or dibiotinylated IGF-2 (Robinson and Rosenzweig, 2004) at 4°C overnight. The membrane was then washed twice in TBS containing 0.2% gelatin at 23°C for 10 min. The blot was incubated for 1 h at 23°C with 8 μg of HRP-NeutrAvidin (Pierce Chemical) in TBS containing 0.2% gelatin. The blot was then exposed to BioMax MR-1 X-ray film (Eastman Kodak, Rochester, NY) for 1 to 30 min. To strip blots, the wet blot was placed in 30 ml of stripping buffer (100 mM Tris, pH 6.7, and 10% SDS) containing 210 μl of β-mercaptoethanol and incubated in a 60°C hybridization oven for 20 min. The stripped blot was washed for 10 min (twice) in TBS with 0.1% Tween 20, followed by blocking for 1 h with bovine lacto-transfer technique optimizer at 23°C and probed with the indicated antibody.

IGFBP-2$_{1–248}$, IGFBP-2$_{1–190}$, and IGFBP-2$_{249–289}$ Expression Constructs. IGFBP-2$_{1–248}$ was generated using oligonucleotides 5′-CGC GGA TCC GAG GTG CTG TTC CGC TGC-3′ and 5′-CCG GAA TTC TTA CCA GCA CTC CCC ACG CTG-3′. IGFBP-2$_{1–190}$ was generated using oligonucleotides 5′-CGC GGA TCC GAG GTG CTG TTC CGC TGC-3′ and 5′-CCG GAA TTC TTA GGG AGT CCT GGC AGG GGG-3′. Polymerase chain reaction (PCR) was performed using the following PCR conditions: initial duration at 95°C for 2 min followed by 30 cycles of 95°C for 30 min, 60°C for 30 s, and 72°C for 60 s. The various IGFBP-2 mutants were cloned without the signal peptide-encoding sequence into the pGEX 6P-1 vector (Amersham Biosciences Inc.) between the BamHI and EcoRI restriction sites in the multiple cloning site.

IGFBP-2$_{249–289}$ was generated using oligonucleotides 5′-GAT CCT GTG TGA ACC CCA ACA CCG GGA AGC TGA TCC AGG GAG CAC CCA CCA TCC GCG GCG ACC CAG AGT GTC ATC TCT TCT ACA ATG AGC AGC AGG AGG CTT GCG GTG TGC ACA CCC AGC GGA TGC AGT AGG-3′ and 5′-GAC ACA CTT GGG GTT GTG GCC CTT CGA CTA GGT CCC TCG TGG GTG GTA GGC GCC GCT GGG TCT CAC AGT AGA GAA GAT GTT ACT CGT CGT CCT CCG AAC GCC ACA CGT GTG GGT CGC CTA CGT CAT CCT TAA-3′. These oligonucleotides were annealed using the following PCR conditions: initial duration at 95°C for 30 s followed by 29 cycles of 53°C for 45 s, and 72°C for 90 s. The annealed DNA was incubated with DNA polymerase I large fragment (Klenow; New England Biolabs) to fill in the 3′ ends. The PCR products were blunt-ended using Zero Blunt TOPO PCR cloning kit (Invitrogen, Carlsbad, CA). A stop codon (TGA) that was introduced during this procedure was changed to GGA using QuikChange site-directed mutagenesis kit (Stratagene, La Jolla, CA). The mutant was cloned without the signal peptide-encoding sequence into the pGEX 6P-2 vector (Amersham Biosciences Inc.) between the BamHI and EcoRI restriction sites in the multiple-cloning site.

Bacterial Expression. Constructs were transformed into the Origami B (DE3) LysS strain of *E. coli* (Novagen, Madison, WI), and the cells were incubated at 37°C in 10 ml of Luria-Bertani medium containing 50 μg/ml ampicillin and 1 g/100 ml of glucose. After a 100-fold dilution into fresh Luria-Bertani medium/ampicillin, the cells were regrown to mid-log phase ($E_{600\ nm}$ = ~0.6), the expression of the proteins, as glutathione *S*-transferase fusion proteins, was induced by addition of 1 mM isopropyl β-D-thiogalactoside at 37°C for 2 to 3 h. Cells were harvested by centrifugation at 4000 rpm for 20 min. The samples were subjected to a freeze-thaw cycle to lyse the cells followed by suspension in lysis buffer. After 15-min incubation on ice, lysis was completed by three 20-s cycles of sonication with cooling on ice for 20 min to allow for solubilization. Insoluble material was removed by centrifugation at 4000 rpm for 20 min, twice. The protein was expressed originally in the Origami B strain of *E. coli*. However, after subsequent tests, we produced the protein in the BL21 (DE3) strain of *E. coli* as a result of higher yields. The protein behaved the same (data not shown).

Purification of IGFBP-2 Fragments. Supernatants from each lysate were incubated at 23°C for 30 min with a 50% slurry of equilibrated glutathione-Sepharose 4B (Amersham Biosciences Inc.; 1-ml bed volume per 100 ml of sonicate). The fusion protein-bound matrix was collected by centrifugation at 500*g* for 5 min and washed three times with 10 bed volumes of phosphate-buffered saline. It was further washed three times with 10 bed volumes of high (25 mM HEPES, 0.05% NaN_3, 0.5 M NaCl, and 0.1% Triton X-100, pH 7.5) and low (25 mM HEPES, 0.05% NaN_3, 0.1 M NaCl, and 0.1% Triton X-100, pH 7.5) salt. The matrix was then equilibrated in PreScission Protease cleavage buffer (50 mM Tris-HCl, pH 7.5, 150 mM NaCl, and 1 mM EDTA) at 4°C. The residual buffer was removed, and the IGFBP-2 fragments were eluted by release (cleavage) from GST bound to the glutathione-Sepharose 4B beads. For each milliliter of washed glutathione-Sepharose bed volume, 40 μl (80 units) of PreScission Protease (cleaves at Q-G bonds and is also a GST fusion protein; Amersham Biosciences Inc.) were mixed with 960 μl of cleavage buffer, added to the fusion protein-bound glutathione-Sepharose, and gently suspended. It was incubated while nutating at 4°C for 4 h. The eluate, containing the protein of interest, was collected by centrifugation of bulk glutathione-Sepharose matrix at 500*g* for 5 min. Then, 200 μl of IGF-1-Sepharose was added to the eluate and was nutated at 23°C for 1 h. It was then placed at 4°C, nutating overnight, followed by nutating for 1 h at 23°C. It was washed three times at 23°C with AC buffer (50 mM HEPES, 150 mM NaCl, and 0.05% NaN_3, pH 7.4) and 0.1× AC buffer. The protein was eluted using 0.5 M acetic acid (except IGFBP-2$_{249–289}$). The truncation mutants were resolved on 12.5% SDS-polyacrylamide gels. Concentrations of the protein were assessed by densitometry of Coomassie-stained SDS gels using NIH Image (version 1.61). This method was validated by amino acid analysis (to within 9.25%).

6His-IGFBP-2 Expression Construct. pET15b 6His-IGFBP-2 was cloned via PCR using CMV-IGFBP-2 as a template and the following primers: 5′-CGC CTC GAG GTG CTG TTC CGC TGC-3′ and 5′-CCG GGA TCC TTA CTG CAT CCG CTG-3′. The PCR product of ~875 bp corresponding to the sequence of the mature protein, minus the signal sequence, was gel purified by agarose electrophoresis and digested with XhoI and BamHI. The oligonucleotide was then ligated into the pET15b vector (Novagen), which had previously been digested with XhoI and BamHI. Confirmation of the correct clone was made by DNA sequencing.

Bacterial Expression of 6His-IGFBP-2. The 6His-IGFBP-2 construct was transformed into BL21 (DE3) *E. coli*, and the cells were incubated at 37°C in 10 ml of Luria-Bertani medium containing 200 μg/ml ampicillin. After a 100-fold dilution into fresh Luria-Bertani medium/ampicillin, the cells were regrown to mid-log phase ($E_{600\ nm}$ = ~0.6), and the expression of the protein was induced by addition of 1 mM isopropyl β-D-thiogalactoside at 37°C for 3 h. Cells were harvested by centrifugation at 4000 rpm for 20 min. The samples were subjected to freeze-thaw cycle to lyse the cells.

Purification of 6His-IGFBP-2. Supernatants from each lysate were incubated at 4°C for 1 h with 50% slurry of equilibrated His-Select nickel affinity gel (Sigma-Aldrich). The protein-bound beads were collected by centrifugation at 500*g* for 5 min and washed three times with His-equilibration buffer (50 mM sodium phosphate and 0.3 M sodium chloride, pH 8.0). They were further washed three times with 10 bed volumes of high (25 mM HEPES, 0.05% NaN_3, 0.5 M NaCl, and 0.1% Triton X-100, pH 7.5) and low (25 mM HEPES,

0.05% NaN_3, 0.1 M NaCl, and 0.1% Triton X-100, pH 7.5) salt. The beads were then washed three times with 5 mM imidazole in His-equilibration buffer. The protein was eluted with 200 mM imidazole in His-equilibration buffer. After elution, the imidazole was dialyzed away overnight at 4°C against AC buffer. The sample was then collected and placed over IGF-1-Sepharose as detailed above.

IGFBP-$2_{249–289}$ Binding Assay. The indicated concentrations of competing, unlabeled IGFBP-$2_{249–289}$ (0–887 nM) were added to a constant amount of IGFBP-2 (0.3 pM) and ^{125}I-IGF-1 (20,000 cpm; 15 pM). Afteran overnight incubation at 4°C, 200 μl of 0.5% bovine gamma globulin was added, followed by 400 μl of 25% PEG. The samples were incubated for 10 min at 23°C and centrifuged for 15 min at 15,000*g*. The pellets were washed with 1 ml of 6.25% PEG, and bound radioactivity (^{125}I-IGF-1 bound to IGFBP-2) was quantified in a Compugamma spectrometer (LKB-Wallac).

SCC-9 Cell Culture. SCC-9 cells (human squamous cell carcinoma cell line of the tongue) purchased from American Type Culture Collection (Manassas, VA) were routinely maintained in a 1:1 mixture of Dulbecco's modified Eagle's medium/Ham's F-12 medium supplemented with 10% fetal bovine serum, 10 ml/l penicillin/streptomycin, 2.38 g/l HEPES, sodium bicarbonate (1.176 g/l for Ham's F-12; 3.70 g/l for Dulbecco's modified Eagle's medium), and 400 ng/ml hydrocortisone at 37°C in an atmosphere of 95% air, 5% CO_2 in a humidified incubator.

Cell Binding Assays. SCC-9 were grown to 80% confluence, serum-starved for 24 h, and washed with HMS± (25 mM HEPES, 104 mM NaCl, 5 mM $MgCl_2$, 0.01% soybean trypsin inhibitor, and 0.2% BSA, pH 7.4). Treatments included increasing concentrations of IGFBP-2 or fragment (0.1–500 nM) and ^{125}I-IGF-1 (20,000 cpm). Treatments were preincubated at 37°C for 2 h and then placed on the cells for 30 min at 23°C. The cells were rinsed with HMS±. NaOH was added to dissolve the cells, and the radioactivity was quantified in the gamma counter. Assays were conducted with triplicate concentrations and repeated at least three times.

Association Kinetics Experiments. These experiments were carried out using PEG precipitation and centrifugation. Four nanograms of recombinant human IGFBP-2 or 100 ng of IGFBP-2-truncation mutant were combined with ± 500 nM IGF-1 in binding assay buffer (200 mM HEPES, pH 6.0, 44 mM $NaHCO_3$, 0.1% bovine serum albumin, 0.01% Triton X-100, and 0.02% NaN_3) followed by 20,000 cpm of ^{125}I-IGF-1. At times 0, 5, 15, 30, 60, 120, 180, 240 min, bovine gamma globulin and PEG were added and worked up as described in the competition binding assay method above. Assays were conducted with triplicate concentrations and repeated at least three times.

Dissociation Kinetics Experiments. These experiments were carried out using PEG precipitation and centrifugation. Four nanograms of recombinant human IGFBP-2 or 100 ng of IGFBP-2-truncation mutant was combined with 20,000 cpm of ^{125}I-IGF-1 in binding assay buffer. After 240 min of association, 500 nM IGF-1 was added to each tube (=time 0). At times 5, 15, 30, 60, 120, 180, and 240 min, bovine γ-globulin and PEG were added, and the samples were worked up as described above. Assays were conducted with triplicate concentrations and repeated at least three times.

Results

Production and Validation of IGFBP-2. A representative chromatogram from the final stage of purification is shown in Fig. 2A, including anti-IGFBP-2 immunoblot analysis of the peaks observed (Fig. 2B). As shown in Fig. 2C, MALDI-TOF MS confirmed the presence of a single protein with molecular ion mass 31,453.7 (mol. wt. 31,452.7). In addition to the singly charged molecular ion, the doubly and

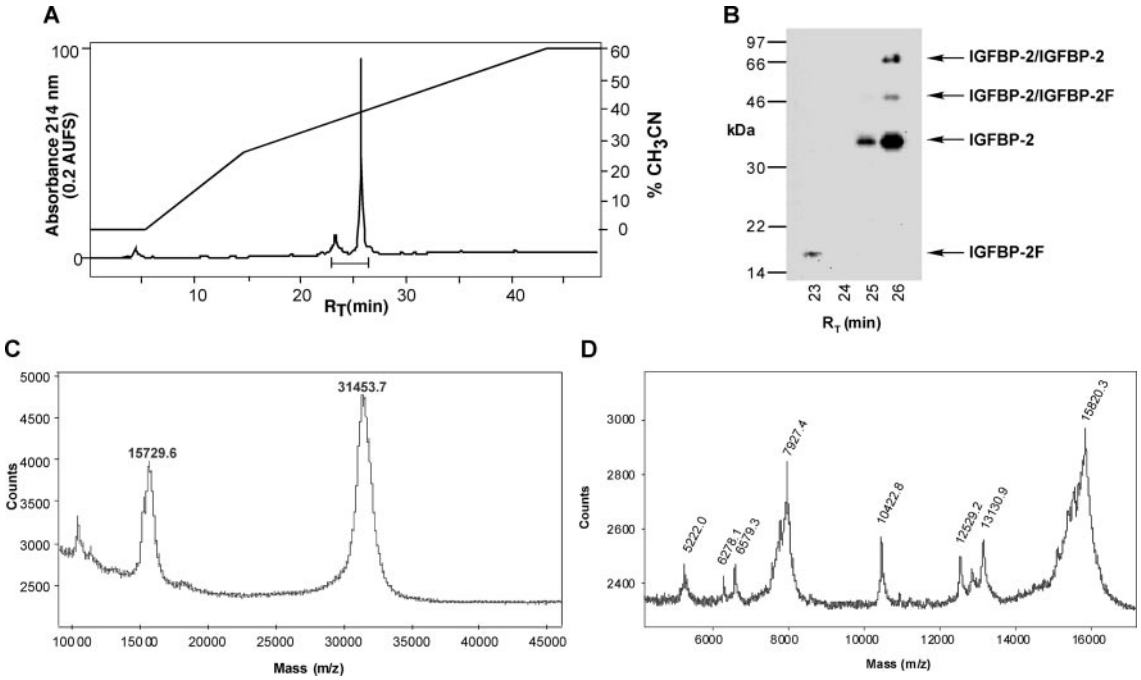

Fig. 2. Purification and analysis of IGFBP-2. Lyophilized CHO-IGFBP2 CM was purified over IGF-1-Sepharose as described under *Materials and Methods*. The eluate was dried in vacuo, dissolved in 0.1% TFA, and injected onto a C4 column. A, typical elution profile. The bars indicate the peaks collected for analysis. B, fractions 23 to 27, collected as two separate peaks from the C4 elution profile shown, were resolved on a 10% SDS gel under nonreducing conditions, transferred to nitrocellulose, and immunoblotted with a polyclonal anti-IGFBP-2 antibody. Intact IGFBP-2 constituted >98% of the peak with retention time (R_T) of 25 to 26 min by densitometric analysis. An ~15.8-kDa band was detected by immunoblot (IGFBP-2F). C, purified IGFBP-2 was subjected to MALDI-TOF MS analysis as described under *Materials and Methods*. Peaks obtained represent the singly $(M + H)^+$, doubly $(M + 2H)^{2+}$, and triply $(M + 3H)^{3+}$ charged states of the molecular ion, with observed *m/z* of 31,453.7, 15,729.6, and 10,487.3, respectively. The predicted mass for IGFBP-2 in the singly charged state is 31,322.7. No other peaks were observed. D, MALDI-TOF MS analysis of IGFBP-2F. The mass peaks obtained represent the singly $(M + H)^+$ and doubly $(M + 2H)^{2+}$ charged states of one major species with observed mass 15,819.3, and three minor species with observed masses 13,129.9, 12,528.2, and 10,421.8. No other mass peaks were observed.

triply charged ions were observed with *m/z* of 15,729.6 (calculated mol. wt. 31,457.2) and 10,487.3 (calculated mol. wt. 31,458.9), respectively. A molecular mass of 31,322.7 Da was expected from the nucleotide sequence of the transfected cDNA. Because the protein contains an uneven number of Cys residues, the mass difference may be because of a Cys residue linked to the additional sulfhydryl group (103 Da) (Feyen et al., 1991). IGFBP-2 was pure based on SDS-PAGE and MALDI-TOF-MS. We used an absorbance value of 0.713 for a 1 mg/ml solution of IGFBP-2 in distilled water to quantify all preparations. In addition to full-length IGFBP-2, a second species capable of binding IGF-1 based on its isolation from the IGF-1-Sepharose column was identified (IGFBP-2F). This ~16-kDa peak was heterogeneous in content (Fig. 2D) and variably observed. It reacted with a polyclonal IGFBP-2 antiserum (Fig. 2B), and it was probably a proteolytic fragment of IGFBP-2 made up of either the C terminus based on its lack of staining with a mid-region-directed antibody and peptide mapping profile (M. J. Horney and S. A. Rosenzweig, unpublished observations). Two heavier components, tentatively identified as an IGFBP-2 homodimer (~66 kDa) and an IGFBP-2/IGFBP-2F heterodimer (~47 kDa), were identified (Fig. 2B). These species were absent from immunoblots run under reducing conditions, supporting the notion that they are disulfide-linked dimers.

Binding and Biologic Activities of IGFBP-2. We next tested the IGF-1 binding affinity and biologic activity of recombinant IGFBP-2 in soluble binding and cell growth inhibition assays, respectively. IGF-1 had an EC_{50} of ~170 pM when competing with ^{125}I-IGF-1 for binding to IGFBP-2 (Fig. 3A). This indicated a K_D of 150 pM for IGFBP-2, approximately 1 order of magnitude higher affinity than the IGF-1R. To assess the biologic activity of recombinant IGFBP-2, we tested its ability to inhibit IGF-1 stimulated and basal growth of human MCF-7 breast cancer cells. As shown in Fig. 3B, IGFBP-2 inhibited IGF-1 stimulated MCF-7 cell proliferation at 20 and 100 nM concentrations. The 20 nM dose reduced the effect of a maximal stimulatory dose of IGF-1 (20 nM) by ~50%. IGFBP-2 (100 nM) reduced the effect of 20 nM IGF-1 by greater than 80%, to near unstimulated growth levels. The lack of complete growth inhibition may be explained by the presence of an endogenous growth-stimulating IGF-2:IGF-1R autocrine loop (Quinn et al., 1996). The existence of an autoregulatory loop is clearly evident in the samples where no exogenous IGF-1 was added. In this case, basal growth was significantly inhibited by addition of either 20 or 100 nM IGFBP-2 to levels below that seen in control cultures (Fig. 3B). The lack of complete blockade of IGF-1 action may be because of proteolysis of IGFBP-2 by proteinases expressed by the MCF-7 cells (E. Eaton and S. Rosenzweig, unpublished observations) (Bunn and Fowlkes, 2003).

BNPS-Skatole Cleavage of IGFBP-2. Based on the properties of BNPS-skatole and the C-terminal disulfide bonding pattern of IGFBP-2 (Forbes et al., 1998), we predicted that the BNPS-skatole reaction products would include IGFBP-$2_{1–248}$ and IGFBP-$2_{249–289}$ with molecular masses of 26,755.6 and 4585.1 Da, respectively (Fig. 4A). Cleavage of IGFBP-2 with BNPS-skatole was examined by immunoblot and ligand blot analyses (Fig. 4B). Using a C-terminal-specific IGFBP-2 antibody, both intact IGFBP-2 and IGFBP-$2_{249–289}$ were detected (Fig. 4B, b). IGFBP-$2_{1–248}$ was not labeled, consistent with the loss of its epitope-containing C terminus (249–289). IGFBP-$2_{249–289}$ migrated according to its predicted molecular mass of ~5 kDa and was faintly stained. Probing with a polyclonal anti-IGFBP-2 antibody revealed the presence of intact IGFBP-2 and IGFBP-$2_{1–248}$ in the final reaction mixture (Fig. 4B, c). IGFBP-$2_{1–248}$ migrated more rapidly than intact IGFBP-2, with an apparent electrophoretic mobility of ~29 kDa, consistent with the loss of its C terminus. The presence of intact IGFBP-2 suggested that the reaction efficiency was considerably less than 100%. To determine the IGF-1 binding activity of the reaction products, ligand blot analysis was used (Fig. 4B, d). Intact IGFBP-2, IGFBP-$2_{1–248}$ and IGFBP-$2_{249–289}$ were all detectable by ligand blot, indicating that they retain IGF-1 binding activity.

Sequence Analysis of IGFBP-2 BNPS-Skatole Cleavage Reaction Products. To confirm the BNPS-skatole

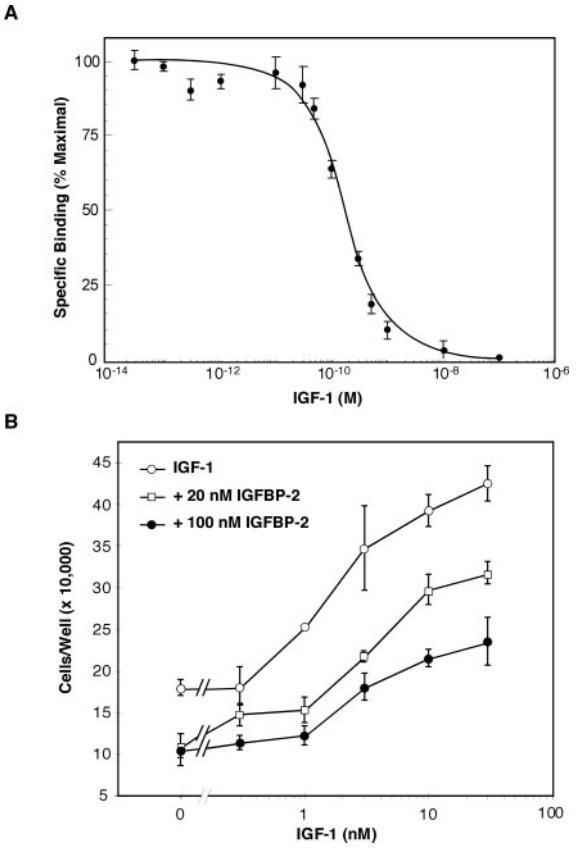

Fig. 3. Competition binding and biologic activity of IGFBP-2. A, IGFBP-2 binding curve. Competition binding assay using increasing doses of IGF-1 in the presence of a fixed amount of ^{125}I-IGF-1 and IGFBP-2. IGFBP-2 (1 ng) was combined with various concentrations of IGF-1 ranging from 30 fM to 100 nM followed by addition of 10 nCi of ^{125}I-IGF-1 (15 pM). After a 4-h incubation at 23°C, 250 μl of 0.5% bovine gamma globulin was added followed by 500 μl of 25% PEG. The samples were incubated for 10 min at 23°C and centrifuged 3 min at 13,000 rpm. The pellets were washed with 1 ml of 6.25% PEG, and bound radioactivity was quantified. Counts bound in the presence of 1 μM IGF-1 (nonspecific binding) were subtracted to obtain specific binding. 100% specific binding is the maximum number of counts bound in the absence of competing ligand (IGF-1) after subtraction of nonspecific counts. Nonspecific counts are counts bound in the presence of a saturating dose of competing ligand (1 μM IGF-1). B, serum-starved MCF-7 cells in 24-well plates were stimulated for 96 h with the indicated concentrations of IGF-1 and IGFBP-2. Cells were trypsinized and counted with a hemocytometer. Shown are average cell numbers for triplicate wells ± S.E. Similar results were obtained in at least three separate experiments.

cleavage specificity the reaction products from an IGFBP-2 BNPS-skatole cleavage reaction were separated by RP-HPLC on a C4 column. Fractions from each peak were collected, resolved by SDS-PAGE, transferred to a microporous PVDF membrane, and stained with Coomassie Brilliant Blue (data not shown). Although intact IGFBP-2 and IGFBP-$2_{1–248}$ coeluted from the column, IGFBP-$2_{249–289}$ eluted as a single component. To confirm their identities, Edman degradation was performed on each band by gas-phase sequencing. The sequence data obtained matches the predicted results (Table 1). These findings, together with the blots shown in Fig. 4, confirm that BNPS-skatole cleaves IGFBP-2 at the C-terminal end of the tryptophan residue in the CWCV motif.

MALDI-TOF MS Analysis of IGFBP-2 BNPS-Skatole Cleavage Reaction Products. To further verify the BNPS-skatole cleavage site on IGFBP-2, the reaction products were resolved by RP-HPLC and analyzed by MALDI-TOF MS (data not shown). The MALDI-TOF MS spectrum of one HPLC fraction exhibited a peak at *m/z* 31,509.6 (theoretical 31,322.7 Da), corresponding to intact IGFBP-2. A second peak in this HPLC fraction and MALDI-TOF MS spectrum was observed at *m/z* 26,806.7. This corresponds to IGFBP-$2_{1–248}$ (theoretical 26,755.6 Da). The MALDI-TOF MS spectrum of another HPLC fraction exhibited a peak with the strongest signal at *m/z* 4720.0. This corresponds to IGFBP-$2_{249–289}$ with a theoretical mass of 4585.1 Da. The differences between the observed and theoretical masses (IGFBP-2, 186.9 Da; IGFBP-$2_{1–248}$, 51.1 Da; and IGFBP-$2_{249–289}$, 134.9 Da) are likely to have ben caused by modifications caused by BNPS-skatole side reactions. The well known BNPS-skatole-induced modifications include conversion of methionine to its sulfoxide (+16 Da), oxidation of C-terminal tryptophan (+14 Da), oxidation of internal tryptophan (+16 Da), and bromination of tyrosine [+79 Da (Vestling et al., 1995; Rahali and Gueguen, 1999)]. Furthermore, other studies using BNPS-skatole have reported the inability to account for an increase of 100 Da of a reaction product (Rahali and Gueguen, 1999). As described above, these results confirm that BNPS-skatole cleaved IGFBP-2 at its tryptophan residue.

Expression and Characterization of 6His-IGFBP-2 and IGFBP-2 Truncation Mutants. Although ligand blot analysis provides qualitative assessments of IGF:IGFBP binding interactions, to obtain a quantitative analysis and define affinities, it is necessary to perform competition binding assays. Given the low yields of product formation using BNPS-skatole and the fact that we obtained a number of potential side reactions leading to chemical modifications of IGFBP-2 and its reaction products, we expressed the predicted products of the BNPS-skatole reaction as well as IGFBP-$2_{1–190}$ as GST-fusion proteins (Fig. 5A; Shand et al., 2003). The truncation mutants were sequentially purified on glutathione-Sepharose, eluted by cleavage with PreScission

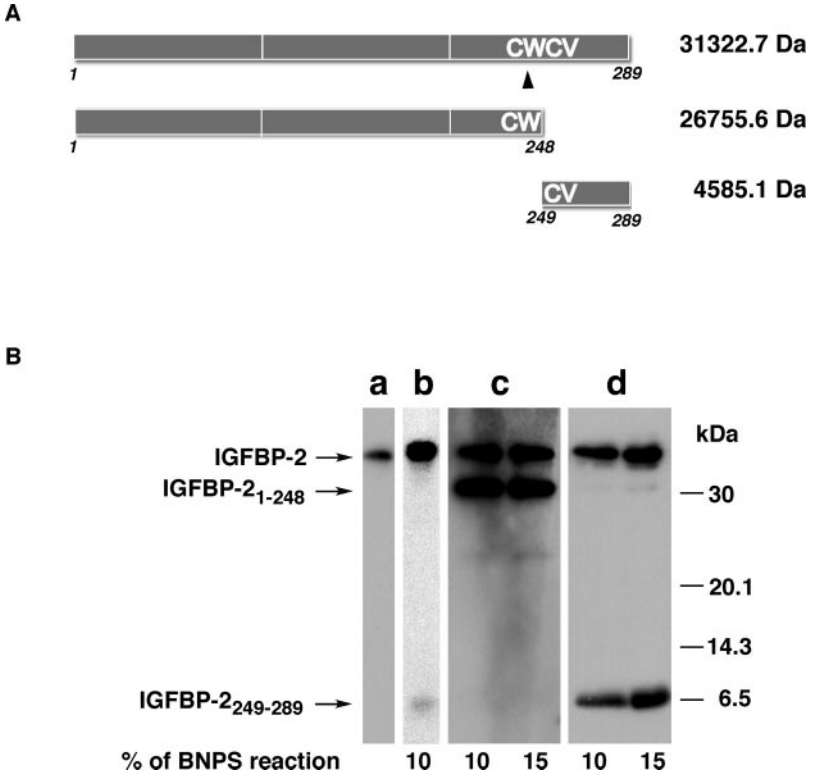

Fig. 4. BNPS-skatole cleavage of IGFBP-2. A, BNPS-skatole cleaves at the C-terminal end of tryptophan residues (Fontana, 1972). The arrowhead designates the predicted site of cleavage within the CWCV motif of IGFBP-2. The theoretical masses are based on the amino acid compositions of the respective proteins and peptides. B, 20 ng of IGFBP-2 (a). Ten percent and 15% of a 10-μg reaction (b–d). Samples were boiled in SDS sample buffer, resolved by SDS-PAGE, transferred to nitrocellulose, and probed with a polyclonal anti-IGFBP-2 antibody (a), a site-specific anti-IGFBP-2 C-terminal antibody (b), or tetrabiotinylated IGF-1 (d) (Robinson and Rosenzweig, 2004). The ligand blot was stripped and reprobed with a polyclonal anti-IGFBP-2 antibody (c). The IGFBP-2 C-terminal-specific antibody labeled intact IGFBP-2 and IGFBP-$2_{249–289}$ (b). With the polyclonal anti-IGFBP-2 antibody, IGFBP-2 and IGFBP-$2_{1–248}$ bands were heavily labeled (c). In the ligand blot (d), IGFBP-2, IGFBP-$2_{1–248}$ and IGFBP-$2_{249–289}$ were detected. The autoradiographs shown are representative of at least three independent experiments.

TABLE 1

Sequence analysis of BNPS-skatole-cleaved IGFBP-2

BNPS-skatole-cleaved IGFBP-2 was separated by RP-HPLC on a C4 column. Fractions from each peak were collected, resolved by SDS-PAGE, transferred to a microporous PVDF membrane, and stained with Coomassie Brilliant Blue. Each band was subjected to gas-phase sequencing.

Result	IGFBP-2	IGFBP-$2_{1–248}$	IGFBP-$2_{249–289}$
Predicted	EVLFRCPPCT	EVLFRCPPCT	CVNPNTGKLI
Sequencing	EVLFRXPPXT	EVLFRXPPXT	XVNPNTGKLI

protease, and subsequently affinity purified on IGF-1-Sepharose (except IGFBP-$2_{249–289}$). Because we could not express IGFBP-2 as a GST-fusion protein, it was cloned into the pET15b vector with an N-terminal 6His-tag. As part of the cloning strategy, a linker containing the amino acids GPLGS was added to all expressed proteins. Furthermore, extra amino acids, PGIRGS and SSGLVPRGSHML, were added at the N terminus of IGFBP-$2_{249–289}$ and 6His-IGFBP-2, respectively, during the cloning process. The added peptides were reflected in the masses obtained by MALDI-TOF MS analysis. MALDI-TOF MS analysis (Fig. 5B) of the purified proteins revealed masses (*m/z*) of 33,337.06 (6His-IGFBP-2; theoretical 33,368.0 Da; a), 27,177.5 (IGFBP-$2_{1–248}$; theoretical 27,167.0 Da; b), 20,357.7 (IGFBP-$2_{1–190}$; theoretical 20,359.2 Da; c), and 5637.1 (IGFBP-$2_{249–289}$; theoretical 5634.3 Da; d), consistent with their purity and expected masses.

Ligand Blot Analysis of IGFBP-2, 6His-IGFBP-2, and IGFBP-2 Truncation Mutants. We initially tested the IGF binding activity of the recombinant proteins using ligand blot analysis with biotinylated IGF-1 or IGF-2 (Fig. 6A). Both IGFBP-$2_{1–248}$ and IGFBP-$2_{1–190}$ bound IGF-2 to a greater extent than IGF-1 as reflected by stronger signals. Furthermore, IGFBP-$2_{1–248}$ exhibited greater IGF binding activity than 1GFBP-$2_{1–190}$. For example, 0.25 μg of IGFBP-$2_{1–248}$ was readily detected with biotinylated IGF-1, whereas only a faint band was detected using 2.5 μg of IGFBP-$2_{1–190}$. The difference in the intensities of the bands in Figs. 4B versus 6B may be because of BNPS-skatole-induced chemical mod-

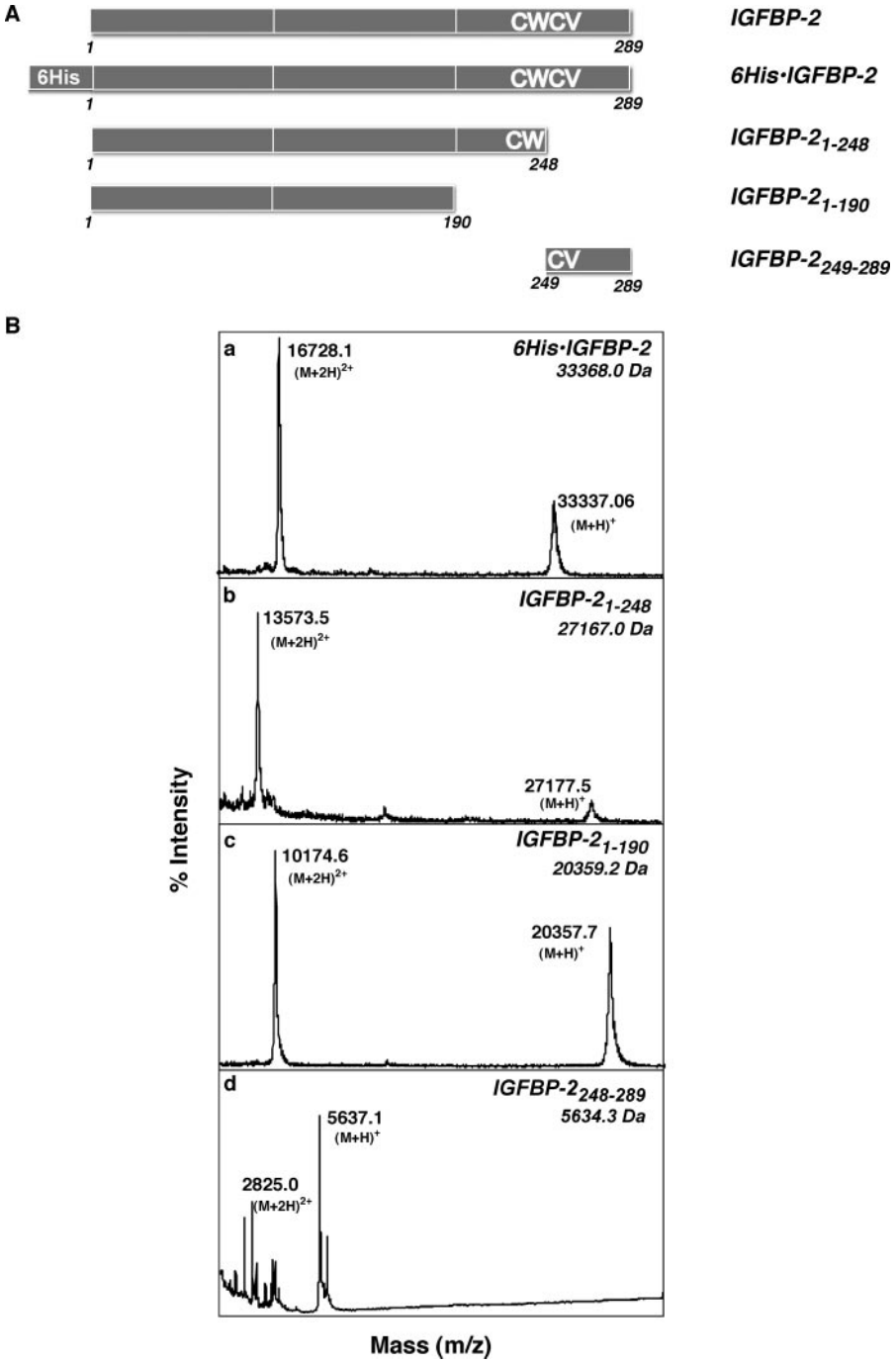

Fig. 5. Characterization of 6His-IGFBP-2 and IGFBP-2 truncation mutants. A, schematic of 6His-IGFBP-2, IGFBP-$2_{1–248}$, IGFBP-$2_{1–190}$, and IGFBP-$2_{249–289}$ expressed in *E. coli*. B, MALDI-TOF MS analysis of 6His-IGFBP-2 (a), IGFBP-$2_{1–248}$ (b), IGFBP-$2_{1–190}$ (c), and IGFBP-$2_{249–289}$ (d). The *y*-axis is 0 to 100% ion intensity, and *x*-axis is *m/z* range 13,000 to 40,000 for 6His-IGFBP-2 (a), *m/z* range 12,000 to 30,000 for IGFBP-$2_{1–248}$ (b), *m/z* range 8500 to 22,000 for IGFBP-$2_{1–190}$ (c), and *m/z* range 1500 to 20,001 for IGFBP-$2_{249–289}$ (d). The mass peaks obtained represent the singly $(M + H)^+$ and doubly $(M + 2H)^{2+}$ charged states of the purified protein. The predicted mass for 6His-IGFBP-2, IGFBP-$2_{1–248}$, IGFBP-$2_{1–190}$, and IGFBP-$2_{249–289}$ in the singly charged state are 33,368.0 (a), 27,167.0 (b), 20,359.2 (c), and 5634.3 (d), respectively.

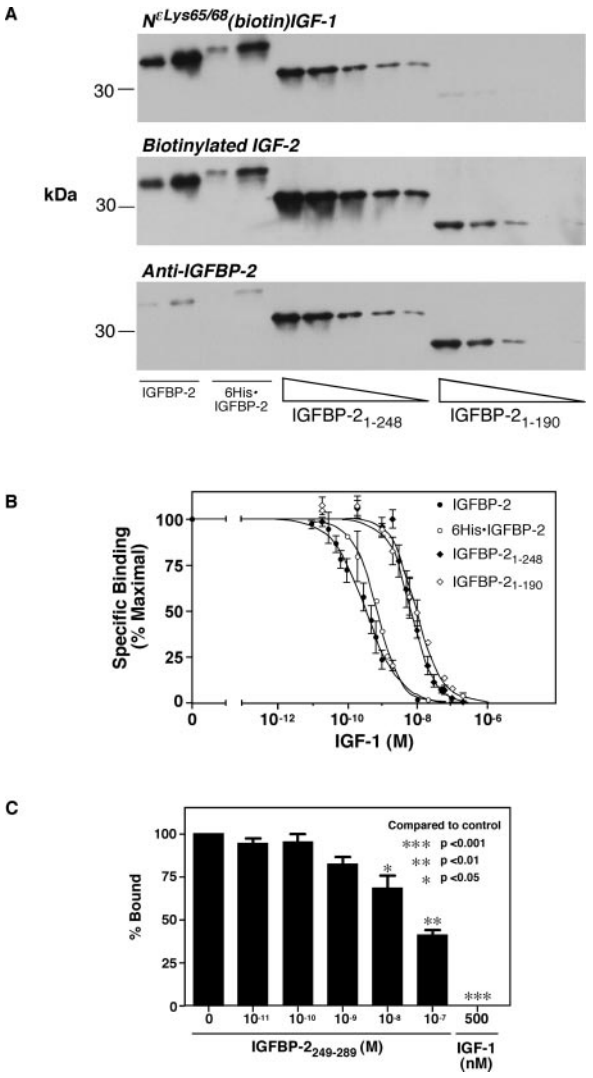

Fig. 6. IGF-1 binding activities of IGFBP-2, 6His-IGFBP-2, and IGFBP-2 truncation mutants. A, ligand blot and immunoblot analyses. Lane 1, 20 ng of IGFBP-2; lane 2, 100 ng of IGFBP-2; lane 3, 20 ng of 6His-IGFBP-2; lane 4, 100 ng of 6His-IGFBP-2. For IGFBP-$2_{1–248}$ and IGFBP-$2_{1–190}$, the following amounts were loaded: 5, 2.5, 1, 0.5, and 0.25 μg. Samples were boiled in SDS sample buffer, resolved by SDS-PAGE, transferred to nitrocellulose, and probed with $N^{\varepsilon Lys\text{-}65/68}$(biotin)-IGF-1, stripped and re-probed with dibiotinylated IGF-2 followed by a polyclonal anti-IGFBP-2 antibody. Autoradiographs shown are representative of at least two independent experiments. B, competition binding assay using increasing doses of IGF-1 in the presence of a fixed amount of ^{125}I-IGF-1 and IGFBP-2, 6His-IGFBP-2, IGFBP-$2_{1–248}$, or IGFBP-$2_{1–190}$. Binding activities were analyzed using a PEG precipitation-based assay to separate bound from free ^{125}I-IGF-1 as described under *Materials and Methods*. IGFBP-2 (4 ng), 6His-IGFBP-2 (4 ng), IGFBP-$2_{1–248}$ (100 ng), or IGFBP-$2_{1–190}$ (100 ng) were combined with various concentrations of IGF-1 (0–100 nM) followed by addition of 10 nCi of ^{125}I-IGF-1 (15 pM). Maximal binding for IGFBP-2 was 6000 cpm, 6His-IGFBP-2 was 5000 cpm, IGFBP-$2_{1–248}$ was 3000 cpm, and IGFBP-$2_{1–190}$ was 3000 cpm. Nonspecific binding was typically ~250 cpm or less than 9% of total binding. The EC_{50} of IGFBP-2 was 0.35 nM, 6His-IGFBP-2 was 0.76 nM, IGFBP-$2_{1–248}$ was 7 nM, and IGFBP-$2_{1–190}$ was 9.2 nM. Prism version 4 (GraphPad Software Inc, San Diego, CA) was used to minimize the sum of the squares of the differences from the mean EC_{50} values for each concentration of IGF-1. Assays were conducted with triplicate concentrations and repeated at least three times for each protein. C, unlabeled IGFBP-$2_{249–289}$ (0–887 nM) was added to a constant amount of IGFBP-2 (0.3 nM) and ^{125}I-IGF-1 (15 pM). After an overnight incubation at 4°C, samples were precipitated with PEG as described under *Materials and Methods*. One hundred precent specific binding is the maximum number of counts bound in the absence of competing ligand (IGFBP-$2_{249–289}$) after subtraction of nonspecific counts. Nonspecific counts are the counts bound in the presence of a saturating dose of IGF-1 (500 nM). Maximal binding for IGFBP-2 was 3800 cpm. Nonspecific binding was typically ~120 cpm or less than 3% of total binding. The EC_{50} for IGFBP-$2_{249–289}$ was 825 nM. Prism version 4 was used to minimize the sum of the squares of the differences from the mean EC_{50} values for each concentration of IGFBP-$2_{249–289}$. Assays were conducted with triplicate concentrations and repeated two times.

ifications. It is noteworthy that6His-IGFBP-2 behaved equivalently to mammalian cell-derived IGFBP-2 (20 and 100 ng).

Competition Binding Studies of IGFBP-2, 6His-IGFBP-2, and IGFBP-2 Truncation Mutants. As illustrated in Fig. 6B, IGFBP-$2_{1–248}$ and IGFBP-$2_{1–190}$ exhibited IGF-1 binding affinities of 7 and 9.2 nM, respectively, for IGF-1. This represents an approximate 20- and 26-fold loss of binding activity compared with intact IGFBP-2 (EC_{50} 0.35 nM). These relatively high affinities contrasted with the comparatively weak signals obtained in ligand blot analysis (Fig. 6, A and B), underscoring the qualitative nature of ligand blotting. This difference could be because of the fact that the competition binding assay is performed in solution, whereas in the ligand blot, proteins are immobilized on nitrocellulose paper. 6His-IGFBP-2 (EC_{50} 0.76 nM) had an affinity for IGF-1 that was comparable with mammalian-cell derived IGFBP-2, indicating that the protein expressed in bacteria was correctly folded. This validates the data collected using proteins expressed in bacteria, with the differences observed being because of altered specificities. To analyze the binding activity of IGFBP-$2_{249–289}$, we had to modify our assay protocol. The assay used PEG precipitation of IGFBP-2 (~32 kDa) and the fact that free, unbound IGF-1 (7.6 kDa) is not precipitated. Owing to its small mass, IGFBP-$2_{249–289}$ (5.6 kDa) is not precipitated by PEG. Thus, we carried out our standard assay, holding IGFBP-2 and ^{125}I-IGF-1 constant and added increasing concentrations of fragment as competitor (Fig. 6C). In this assay, IGFBP-$2_{249–289}$ exhibited an EC_{50} of 825 nM. This differed from the strong signal obtained in ligand blot analysis (Fig. 4B). It is possible that the BNPS-skatole-induced side reactions preferentially modified IGFBP-$2_{249–289}$ (observed theoretical difference of 134.9 Da), enhancing its ability to bind or retain bound IGF-1 in the ligand blot, whereas not affecting or even hindering IGF-1 binding to IGFBP-$2_{1–248}$ (observed theoretical difference of 51.1 Da). In this regard, IGFBP-$2_{249–289}$ lacked binding activity in an immunoprecipitation-based binding assay and when tested in ligand blot analysis (data not shown).

Cell Binding Studies of IGFBP-2, 6His-IGFBP-2, and IGFBP-2 Truncation Mutants. We tested the ability of IGFBP-2, 6His-IGFBP-2, IGFBP-$2_{1–248}$, IGFBP-$2_{1–190}$, and IGFBP-$2_{249–289}$ to inhibit ^{125}I-IGF-1 binding to the IGF-1R in SCC-9 cells (Fig. 7). IGFBP-2 and 6His-IGFBP-2 significantly inhibited IGF-1 binding to the IGF-1R, with a 10 nM dose causing ~80 and 90% inhibition, respectively (Fig. 7A). IGFBP-$2_{1–248}$ (500 nM) significantly inhibited ^{125}I-IGF-1 binding to the IGF-1R (~65%; Fig. 7B), whereas IGFBP-$2_{1–190}$ did not significantly inhibit IGF-1R binding at the doses tested. However, there was a trend; as the concentration of IGFBP-$2_{1–190}$ increased, there was a decrease in the ability of ^{125}I-IGF-1 to bind to the IGF-1R. IGFBP-$2_{249–289}$ did not affect IGF-1 binding (Fig. 7B).

Kinetic Studies of IGFBP-2, 6His-IGFBP-2, and IGFBP-2 Truncation Mutants. The inability of IGFBP-$2_{1–248}$ and IGFBP-$2_{1–190}$ to effectively block IGF-1 binding to

the IGF-1R suggested a significant difference between these truncation mutants and the full-length protein. Hence, we carried out kinetic analyses, comparing the IGF-1 association and dissociation rates for IGFBP-2, 6His-IGFBP-2, IGFBP-$2_{1–248}$, and IGFBP-$2_{1–190}$ (Fig. 8). ^{125}I-IGF-1 associated faster with both truncation mutants compared with IGFBP-2 and 6His-IGFBP-2 ($t_{1/2}$ = 24.7, 25.7, 3.6, and 4.8 min for IGFBP-2, 6His-IGFBP-2, IGFBP-$2_{1–248}$, and IGFBP-$2_{1–190}$, respectively; Fig. 8, left). These data indicated that loss of residues 249 to 289 results in a more rapid association with IGF-1. Deletion of residues 191 to 248 had little further effect on the association/dissociation rates. IGFBP-2 and 6His-IGFBP-2 had similar association/dissociation kinetics. It is noteworthy thatIGFBP-2 had significantly slower dissociation kinetics ($t_{1/2}$ = 16 min) than either truncation mutant, with ~72% of the bound IGF-1 remaining after 4 h (Fig. 8, right). In contrast, greater than 85% of bound IGF-1 dissociated from IGFBP-$2_{1–248}$ within a $t_{1/2}$ of 2 min. Removal of the remainder of the C terminus (191–248) had no further effect. The dissociation rate for 6His-IGFBP-2 was similar to IGFBP-2, with ~84% of bound ligand remaining after 4 h.

Discussion

A renewed interest in the role of the IGF system in cancer has surfaced over the past few years with IGF-1/2 having been identified as risk factors in breast, prostate, colon, cervical (Voskuil et al., 2005), and head and neck cancers (Wu et al., 2004). Accompanied by this is the observation that IGFBP-3 is a negative risk factor for cancer (Rosenzweig, 2004). Based on the premise that the IGFBPs represent natural antagonists of the IGFs, our laboratory is developing IGFBP-mimetics as cancer therapeutics, using IGFBP-2 as a template. The role of the IGFBPs in the onset, development, progression, and aggressiveness of cancer has been challenged in recent years. This, in large part, is based on accumulating literature demonstrating that some IGFBPs have direct stimulatory or inhibitory actions on tumor cells independent of their IGF-sequestering, IGF-1R-inhibiting actions. These intrinsic activities vary according to binding protein and whether normal or cancer cells are under examination (for review, see Rosenzweig, 2004). For example, IGFBP-2 was reported to modestly suppress normal prostate cell growth and potently stimulate prostate cancer cell growth (Moore et al., 2003). Lee et al. (2005) showed that IGFBP-2 enhances the invasion capacity of ovarian cancer cells, and other groups have shown IGF-independent effects in cancer cells (Hoeflich et al., 2001), including stimulatory effects of IGFBP-2 on MCF-7 cell growth (Chen et al., 1994). As depicted in Fig. 3, we only observed inhibition of IGF-1/2 effects. IGFBP-2-related changes in cell growth/tumorigenicity may be the result of integrin engagement by the RGD motif (Pereira et al., 2004). It is noteworthy that we have

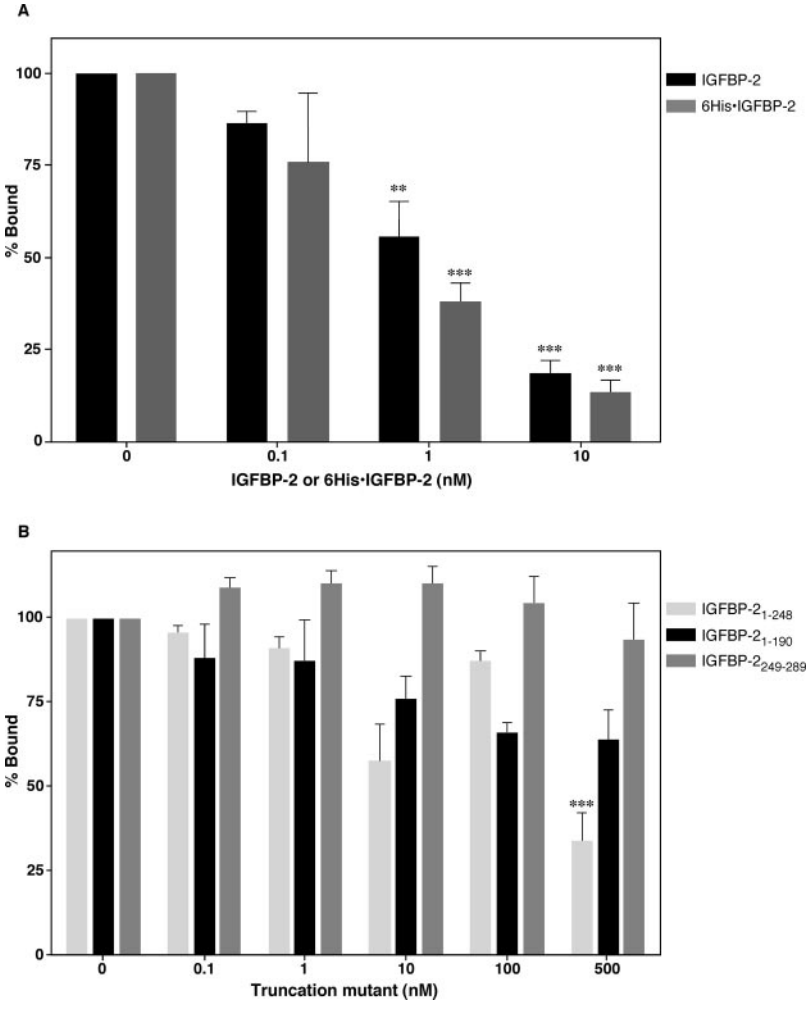

Fig. 7. Inhibition of IGF-1 binding to cells. SCC-9 cells were grown to 80% confluence, serum-starved for 24 h, and washed with HMS±. Increasing doses of IGFBP-2 (A), 6His-IGFBP-2 (A), IGFBP-$2_{1–248}$ (B), IGFBP-$2_{1–190}$ (B), or IGFBP-$2_{249–289}$ (B) plus 20,000 cpm of ^{125}I-IGF-1 was incubated at 37°C for 2 h and then added to the cells for 30 min at 23°C. Cells were rinsed, dissolved in NaOH, and the radioactivity was quantified by gamma spectrometry. Assays were conducted with triplicate concentrations and repeated at least three times. Compared with control ***, $p < 0.001$; **, $p < 0.01$; *, $p < 0.05$.

observed no alterations in cell growth by CHO cells overexpressing IGFBP-2.

We observed the dose-dependent inhibition by IGFBP-2 of MCF-7 cell proliferation in response to exogenously added IGF-1. IGFBP-2 inhibited basal MCF-7 cell growth responses, attributable to blockade of an autocrine IGF-2: IGF-1R growth loop (Quinn et al., 1996). It is likely that autocrine release of IGF-2 is responsible for the lack of a 1:1 M inhibition of exogenous IGF-1 observed, becauseIGF-2 has a higher affinity for IGFBP-2 than IGF-1 and a lower efficacy at the IGF-1R than IGF-1 (Jones and Clemmons, 1995). These results point to an IGF-dependent mechanism of action for IGFBP-2.

6His-IGFBP-2 represents the first expression of high-affinity, full-length human IGFBP-2 in bacteria. Our studies indicate that both the *E. coli*- and mammalian cell-derived IGFBP-2 exhibit the same affinities for IGF-1, kinetics of association/dissociation, and efficacies for inhibiting ^{125}I-IGF-1 binding to cells. Therefore, 6His-IGFBP-2 serves as a key control for the truncation mutants expressed in bacteria and validates our analyses using CHO cell-expressed IGFBP-2.

Using BNPS-skatole, a tryptophan-selective cleavage reagent, we obtained initial evidence that the region downstream of the CWCV motif of IGFBP-2 may contribute to high-affinity IGF-1 binding activity. Owing to side reactions and low yields, BNPS-skatole was useful for obtaining structural information but not for functional analysis of the IGFBPs. To further validate these findings, binding analyses were carried out with IGFBP-$2_{1–248}$ (EC_{50} = 7 nM) which

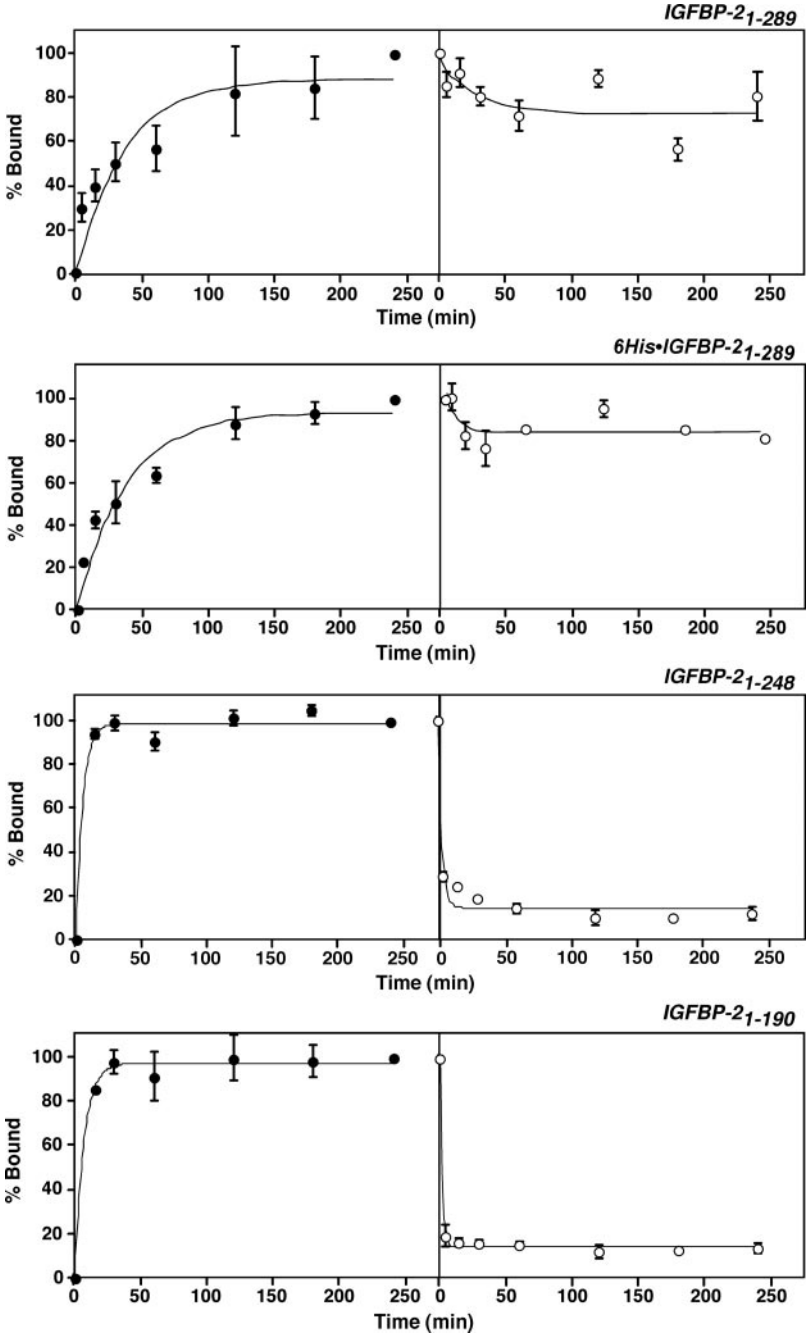

Fig. 8. IGFBP binding kinetics. IGFBP-2 (4 ng), 6His-IGFBP-2 (4 ng), IGFBP-$2_{1–248}$ (100 ng), or IGFBP-$2_{1–190}$ (100 ng) plus 20,000 cpm of ^{125}I-IGF-1 was combined and allowed to bind at 23°C. Left, association kinetics. At the times indicated, aliquots were taken, and the binding was terminated by PEG precipitation and centrifugation. Nonspecific binding (counts bound in the presence of 1 μM IGF-1) was subtracted from all samples. Right, dissociation kinetics. A binding assay was carried out as described above for 240 min, at which time 500 nM IGF-1 was added to initiate the dissociation experiment (time = 0 min). At the times indicated, aliquots were taken and binding was terminated by PEG precipitation and centrifugation. Assays were conducted in triplicate and repeated at least three times.

exhibited an ~20-fold reduction in binding activity compared with intact IGFBP-2 (EC_{50} = 0.35 nM). Reports from other laboratories have also documented a role for the C terminus of IGFBP-2 in IGF binding. Wang et al. (1988) and Ho and Baxter (1997) demonstrated that C-terminal IGFBP-2 fragments (residues 148–270, 169–289, and 181–289) exhibit high-affinity IGF binding activity. Furthermore, Mark et al. (2005) identified a naturally occurring fragment of IGFBP-2 (167–279) from human plasma having 10% of the IGF-2 binding activity of intact IGFBP-2.

IGFBP-$2_{1–190}$ had a binding affinity and kinetic properties that were indistinguishable from those of IGFBP-$2_{1–248}$. The principal differences between these proteins were that IGFBP-$2_{1–190}$ had a lower capacity to block ^{125}I-IGF-1 binding to cells (Fig. 7B) and yielded a weaker signal in ligand blot analyses (Fig. 6A). The present findings corroborate the N-terminal domain as the site of high-affinity IGF binding activity, given the high affinity for IGF-1 exhibited by IGFBP-$2_{1–190}$ (Siwanowicz et al., 2005). Residues upstream of the CWCV motif have been implicated in IGF binding activity by our laboratory (Fig. 1; Horney et al., 2001) and others. Carrick et al. (2001) showed that bovine IGFBP-2 (residues 1–185) had an ~48-fold reduction in IGF binding compared with intact IGFBP-2. They recently reported the NMR structure of bovine IGFBP-2 (Carrick et al., 2005) and demonstrated that the C-terminal domain plays a key role in IGF binding and inhibition of IGF binding to the IGF-1R. These results are in keeping with previous studies that identified residues 222 to 236 of bovine IGFBP-2 to be important for IGF binding (Fig. 1; Forbes et al., 1998). Likewise, mutation of residues Gly-211 and Glu-217 of rat IGFBP-2 resulted in a 4.5-fold reduction in IGF-1 binding activity (Fig. 1; Shand et al., 2003). Finally, using NMR analyses, Bach et al. (2005) reported that residues upstream of the CWCV motif comprise the IGF-2 binding site within the C-terminal domain of IGFBP-6.

To date, IGF cell binding studies have not been performed using IGFBP-2 fragments. Therefore, we tested the ability of the truncation mutants to inhibit IGF-1 binding to the IGF-1R (Fig. 7). Although the IGF-1 binding affinity of IGFBP-$2_{1–248}$ was high (EC_{50} = 7 nM), it exhibited a disproportionate loss in its ability to inhibit IGF-1 binding to the IGF-1R compared with IGFBP-2 (10 versus 500 nM). Likewise,IGFBP-$2_{1–190}$ (EC_{50} = 9.2 nM) had a lower ability than that of IGFBP-$2_{1–248}$ to inhibit IGF-1 binding to cells, requiring higher doses to obtain equivalent inhibition. The finding that IGFBP-$2_{1–248}$ and IGFBP-$2_{1–190}$ had reduced abilities to inhibit IGF-1 binding to the IGF-1R on cells compared with full-length IGFBP-2 was a surprise, given their high affinities for IGF-1. To explain this discrepancy, we carried out kinetic analyses.

Kinetic studies indicated that the region downstream of the CWCV motif (249–289) provides stability to the IGFBP-2/IGF-1 complex, accounting for the slow dissociation rates observed (Fig. 8). When present (IGFBP-2), ~72% of IGF-1 remains bound after 4 h of incubation; when deleted (IGFBP-$2_{1–248}$), ~85% of the bound ligand dissociates within 5 min of incubation. Our results also suggest that the region upstream of the CWCV motif is important for maintaining IGF-1 binding and for contributing to binding efficacy. Our data are consistent with the work of Carrick et al. (2001) who showed that C-terminal deletion mutants of bovine IGFBP-2 (residues 1–185) had faster association and dissociation rates compared with bovine IGFBP-2His (residues 1–279). The similar association/dissociation rates of IGFBP-$2_{1–248}$ and IGFBP-$2_{1–190}$ combined with the cell binding data suggest that the region upstream of the CWCV motif (residues 191–248) contribute to blocking IGF-1 from binding to the IGF-1R. Deletion of the entire C-terminal domain significantly reduces the ability to block IGF-1 action. The equivalent affinity and binding kinetics observed for IGFBP-2 and 6His-IGFBP-2 indicate that the N-terminal 6His-tag and linker peptide do not significantly affect IGF-1 binding association, dissociation, or efficaciousness.

These data extend our previous findings (Horney et al., 2001) where we demonstrated that the N-terminal Gly-1 residue on IGF-1 contacts the C-terminal domain of IGFBP-2, supporting the C terminus of IGFBP-2 as an IGF-1 contact site. Using two photoprobes, differing by 3.8 Å (12.8 and 9 Å) in spacer length between the Gly-1 α-amino group of IGF-1 and their reactive nitrenes, two contact sites at 212 to 227 and 266 to 287 were labeled (Fig. 8A). Sala et al. (2005) reported that His-213, an iron (II)-binding residue of IGFBP-1, is important for IGF-2 binding (Fig. 9a). The equivalent residue in IGFBP-2, Asn-232, resides within ~10.3 and ~9.3 Å from residues within the contact sites, measuring from His-221 and Pro-268, respectively (Fig. 9b). This suggests that these two regions may be in close apposition in three-dimensional space and that the Gly-1 residue, which marks the periphery of the IGFBP-binding domain (residues 1–3 and 49–51), may localize within a pocket delineated by residues 227 to 241 (residues equivalent to bovine IGFBP-2 222–236; Fig. 8A; Forbes et al., 1998). Figure 9 demonstrates that IGF-1 can contact the entire C-terminal domain providing a rationale of how loss of the distal C terminus leads to the observed activities.

In summary, this study has demonstrated that IGFBP-2

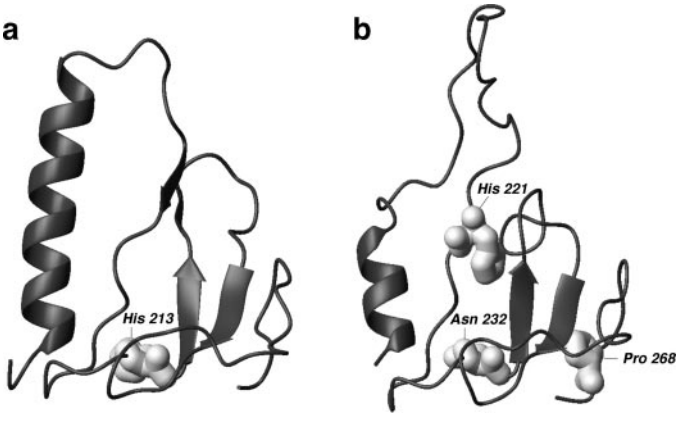

Fig. 9. Thyroglobulin type-1 domain of IGFBP-2. a, backbone representation of the crystal structure of the C-terminal domain of IGFBP-1 (residues 172–251; Protein Data Base code 1ZT3); space-filled residue, His-213 (Sala et al., 2005). b, homology model of the thyroglobulin type-1 domain of IGFBP-2 with the major histocompatibility complex class II-associated p41 fragment (Protein Data Base code 1ICF), using Modeler (http://alto.rockefeller.edu/modbase-cgi/). This domain was first described in major histocompatibility complex class II-associated p41 Ii fragment bound to cathepsin L (Guncar et al., 1999). The modeled segment is 82 amino acids (IGFBP-2, 189–270). Asn-232 (space-filled) is the IGFBP-2 equivalent of His-213 in IGFBP-1 (Sala et al., 2005). Space-filled residues His-221 and Pro-268 are located within the contact sites (212–227 and 266–287) identified by photoaffinity labeling with IGF-1 (Horney et al., 2001). Their distances from Asn-232 are ~10.4 and ~9.3 Å, respectively. This figure was prepared using MOLMOL (Koradi et al., 1996).

acts on MCF-7 cells in an IGF-1 dependent manner, inhibiting IGF-1R stimulated cell proliferation. We also showed that both the distal and proximal regions of the C-terminal domain of IGFBP-2 provide stability and are necessary for inhibiting IGF-1 binding to the IGF-1R, consistent with other IGFBPs (Siwanowicz et al., 2005). These studies support the development of full-length IGFBP-2 as a cancer therapeutic. Future studies will focus on chimeric constructs and IGFBP-2 homologs exhibiting protease resistance and lacking integrin engagement actions.

Acknowledgments

We thank Dr. Kevin Schey and the Medical University of South Carolina Mass Spectrometry Facility for assistance with the analysis of IGFBP-2 and IGFBP-2F and Dr. Benjamin Pettus for help in the cell growth inhibition assays.

References

Bach LA, Headey SJ, and Norton RS (2005) IGF-binding proteins—the pieces are falling into place. *Trends Endocrinol Metab* **16:**228–234.
Binkert C, Landwehr J, Mary JL, Schwander J, and Heinrich G (1989) Cloning, sequence analysis and expression of a cDNA encoding a novel insulin-like growth factor binding protein (IGFBP-2). *EMBO (Eur Mol Biol Organ) J* **8:**2497–2502.
Bunn RC and Fowlkes JL (2003) Insulin-like growth factor binding protein proteolysis. *Trends Endocrinol Metab* **14:**176–181.
Carrick FE, Forbes BE, and Wallace JC (2001) BIAcore analysis of bovine insulin-like growth factor (IGF)-binding protein-2 identifies major IGF binding site determinants in both the amino- and carboxyl-terminal domains. *J Biol Chem* **276:** 27120–27128.
Carrick FE, Hinds MG, McNeil KA, Wallace JC, Forbes BE, and Norton RS (2005) Interaction of insulin-like growth factor (IGF)-I and -II with IGF binding protein-2: mapping the binding surfaces by nuclear magnetic resonance. *J Mol Endocrinol* **34:**685–698.
Chen JC, Shao ZM, Sheikh MS, Hussain A, LeRoith D, Roberts CT Jr, and Fontana JA (1994) Insulin-like growth factor-binding protein enhancement of insulin-like growth factor-I (IGF-I)-mediated DNA synthesis and IGF-I binding in a human breast carcinoma cell line. *J Cell Physiol* **158:**69–78.
Dong F, Wu HB, Hong J, and Rechler MM (2002) Insulin-like growth factor binding protein-2 mediates the inhibition of DNA synthesis by transforming growth factor-beta in mink lung epithelial cells. *J Cell Physiol* **190:**63–73.
Feyen JH, Evans DB, Binkert C, Heinrich GF, Geisse S, and Kocher HP (1991) Recombinant human [Cys281]insulin-like growth factor-binding protein 2 inhibits both basal and insulin-like growth factor I-stimulated proliferation and collagen synthesis in fetal rat calvariae. *J Biol Chem* **266:**19469–19474.
Fontana A (1972) Modification of tryptophan with BNPS-skatole (2-(2-nitrophenylsulfenyl)-3-methyl-3-bromoindolenine. *Methods Enzymol* **25:**419–423.
Forbes BE, Turner D, Hodge SJ, McNeil KA, Forsberg G, and Wallace JC (1998) Localization of an insulin-like growth factor (IGF) binding site of bovine IGF binding protein-2 using disulfide mapping and deletion mutation analysis of the C-terminal domain. *J Biol Chem* **273:**4647–4652.
Galanis M, Firth SM, Bond J, Nathanielsz A, Kortt AA, Hudson PJ, and Baxter RC (2001) Ligand-binding characteristics of recombinant amino- and carboxyl-terminal fragments of human insulin-like growth factor-binding protein-3. *J Endocrinol* **169:**123–133.
Guncar G, Pungercic G, Klemencic I, Turk V, and Turk D (1999) Crystal structure of MHC class II-associated p41 Ii fragment bound to cathepsin L reveals the structural basis for differentiation between cathepsins L and S. *EMBO (Eur Mol Biol Organ) J* **18:**793–803.
Hoeflich A, Reisinger R, Lahm H, Kiess W, Blum WF, Kolb HJ, Weber MM, and Wolf E (2001) Insulin-like growth factor-binding protein 2 in tumorigenesis: protector or promoter? *Cancer Res* **61:**8601–8610.
Ho PJ and Baxter RC (1997) Characterization of truncated insulin-like growth factor-binding protein-2 in human milk. *Endocrinology* **138:**3811–3818.
Hong J, Zhang G, Dong F, and Rechler MM (2002) Insulin-like growth factor (IGF)-binding protein-3 mutants that do not bind IGF-I or IGF-II stimulate apoptosis in human prostate cancer cells. *J Biol Chem* **277:**10489–10497.
Horney MJ, Evangelista CA, and Rosenzweig SA (2001) Synthesis and characterization of insulin-like growth factor (IGF)-1 photoprobes selective for the IGF-binding proteins (IGFBPs). Photoaffinity labeling of the IGF-binding domain on IGFBP-2. *J Biol Chem* **276:**2880–2889.
Imai Y, Moralez A, Andag U, Clarke JB, Busby WH Jr, and Clemmons DR (2000) Substitutions for hydrophobic amino acids in the N-terminal domains of IGFBP-3 and -5 markedly reduce IGF-I binding and alter their biologic actions. *J Biol Chem* **275:**18188–18194.
Jones JI and Clemmons DR (1995) Insulin-like growth factors and their binding proteins: biological actions. *Endocrine Rev* **16:**3–34.
Kalus W, Zweckstetter M, Renner C, Sanchez Y, Georgescu J, Grol M, Demuth D, Schumacher R, Dony C, Lang K, et al. (1998) Structure of the IGF-binding domain of the insulin-like growth factor-binding protein-5 (IGFBP-5): implications for IGF and IGF-I receptor interactions. *EMBO (Eur Mol Biol Organ) J* **17:**6558–6572.
Kaufman RJ and Sharp PA (1982) Amplification and expression of sequences co-transfected with a modular dihydrofolate reductase complementary DNA gene. *J Mol Biol* **159:**601–621.
Koradi R, Billeter M, and Wuthrich K (1996) MOLMOL: a program for display and analysis of macromolecular structures. *J Mol Graph* **14:**51–55, 29–32.
Lee EJ, Mircean C, Shmulevich I, Wang H, Liu J, Niemisto A, Kavanagh JJ, Lee JH, and Zhang W (2005) Insulin-like growth factor binding protein 2 promotes ovarian cancer cell invasion. *Mol Cancer* **4:**7.
Mark S, Kubler B, Honing S, Oesterreicher S, John H, Braulke T, Forssmann WG, and Standker L (2005) Diversity of human insulin-like growth factor (IGF) binding protein-2 fragments in plasma: primary structure, IGF-binding properties and disulfide bonding pattern. *Biochemistry* **44:**3644–3652.
McCusker RH, Campion DR, and Clemmons DR (1988) The ontogeny and regulation of a 31,000 molecular weight insulin-like growth factor-binding protein in fetal porcine plasma and sera. *Endocrinology* **122:**2071–2079.
Moore MG, Wetterau LA, Francis MJ, Peehl DM, and Cohen P (2003) Novel stimulatory role for insulin-like growth factor binding protein-2 in prostate cancer cells. *Int J Cancer* **105:**14–19.
Payet LD, Wang XH, Baxter RC, and Firth SM (2003) Amino- and carboxyl-terminal fragments of insulin-like growth factor (IGF) binding protein-3 cooperate to bind IGFs with high affinity and inhibit IGF receptor interactions. *Endocrinology* **144:**2797–2806.
Pereira JJ, Meyer T, Docherty SE, Reid HH, Marshall J, Thompson EW, Rossjohn J, and Price JT (2004) Bimolecular interaction of insulin-like growth factor (IGF) binding protein-2 with alphavbeta3 negatively modulates IGF-I-mediated migration and tumor growth. *Cancer Res* **64:**977–984.
Quinn KA, Treston AM, Unsworth EJ, Miller MJ, Vos M, Grimley C, Battey J, Mulshine JL, and Cuttitta F (1996) Insulin-like growth factor expression in human cancer cell lines. *J Biol Chem* **271:**11477–11483.
Rahali V and Gueguen J (1999) Chemical cleavage of bovine beta-lactoglobulin by BNPS-skatole for preparative purposes: comparative study of hydrolytic procedures and peptide characterization. *J Protein Chem* **18:**1–12.
Robinson SA and Rosenzweig SA (2004) Synthesis and characterization of biotinylated forms of insulin-like growth factor-1: topographical evaluation of the IGF-1/IGFBP-2 AND IGFBP-3 interface. *Biochemistry* **43:**11533–11545.
Rosenzweig SA (2004) What's new in the IGF-binding proteins? *Growth Horm IGF Res* **14:**329–336.
Sala A, Capaldi S, Campagnoli M, Faggion B, Labo S, Perduca M, Romano A, Carrizo ME, Valli M, Visai L, et al. (2005) Structure and properties of the C-terminal domain of insulin-like growth factor-binding protein-1 isolated from human amniotic fluid. *J Biol Chem* **280:**29812–29819.
Sambrook J, Fritsch E, and Mamiatis T (1989) *Molecular Cloning: A Laboratory Manual*, Cold Spring Harbor Laboratory Press, Cold Spring Harbor, NY.
Shand JH, Beattie J, Song H, Phillips K, Kelly SM, Flint DJ, and Allan GJ (2003) Specific amino acid substitutions determine the differential contribution of the N- and C-terminal domains of insulin-like growth factor (IGF)-binding protein-5 in binding IGF-I. *J Biol Chem* **278:**17859–17866.
Siwanowicz I, Popowicz GM, Wisniewska M, Huber R, Kuenkele KP, Lang K, Engh RA, and Holak TA (2005) Structural basis for the regulation of insulin-like growth factors by IGF binding proteins. *Structure* **13:**155–167.
Vestling MM, Kelly MA, and Fenselau C (1995) Optimization by mass spectrometry of a tryptophan-specific protein cleavage reaction. *Rapid Commun Mass Spectrom* **9:**1051–1055.
Voskuil DW, Vieling A, van 't Veer LJ, Kampman E, and Rookus MA (2005) The insulin-like growth factor system in cancer prevention: potential of dietary intervention strategies. *Cancer Epidemiol Biomarkers Prev* **14:**195–203.
Wang JF, Hampton B, Mehlman T, Burgess WH, and Rechler MM (1988) Isolation of a biologically active fragment from the carboxy terminus of the fetal rat binding protein for insulin-like growth factors. *Biochem Biophys Res Commun* **157:**718–726.
Wu X, Zhao H, Do KA, Johnson MM, Dong Q, Hong WK, and Spitz MR (2004) Serum levels of insulin growth factor (IGF-I) and IGF-binding protein predict risk of second primary tumors in patients with head and neck cancer. *Clin Cancer Res* **10:**3988–3995.
Zeslawski W, Beisel HG, Kamionka M, Kalus W, Engh RA, Huber R, Lang K, and Holak TA (2001) The interaction of insulin-like growth factor-I with the N-terminal domain of IGFBP-5. *EMBO (Eur Mol Biol Organ) J* **20:**3638–3644.

Address correspondence to: Dr. Steven A. Rosenzweig, Department of Cell and Molecular Pharmacology and Experimental Therapeutics, Medical University of South Carolina, 173 Ashley Ave., P.O. Box 250505, Charleston, SC 29425. E-mail: rosenzsa@musc.edu